Doubly-Hydrated Hexafluoroacetylacetone as a Tetradentate Ligand: Synthesis, Magnetochemistry, and Thermal Transformations of a Mn^{III}_2 Complex

Elisabeth Bouwman, Kenneth G. Caulton,* George Christou,* Kirsten Folting, Christophe Gasser, David N. Hendrickson,* John C. Huffman, Emil B. Lobkovsky, James D. Martin, Philippe Michel, Hui-Lien Tsai, and Ziling Xue

Department of Chemistry and Molecular Structure Center, Indiana University, Bloomington, Indiana 47405, and Department of Chemistry-0506, University of California at San Diego, La Jolla, California 92093-0506

Received April 6, 1993

A convenient synthesis of the doubly-hydrated form of hexafluoroacetylacetone (hfacH) is reported, *viz.* 1,1,1,5,5,5,-hexafluoropentane-2,2,4,4-tetraol ($hfptH_4$; **1**), together with the initial employment of the latter as a ligand. A reaction system in CH_2Cl_2 comprising $[Mn_3O(OAc)_6(py)_3](ClO_4)$, hfacH, $hfptH_4$, and py (py = pyridine) in a 1:6:1.5:9 ratio leads to a 58% yield of $(pyH)_2[Mn_2(hfpt)(hfac)_4]$ (**2**). Crystal data for **1** at −171 °C: monoclinic, $P2_1/n$, a = 11.108(6) Å, b = 5.104(3) Å, c = 14.736(8) Å, β = 90.30(2)°, Z = 4, V = 835.44 Å^3, R (R_w) = 6.58% (7.42%). Crystal data for **2** at −130 °C: monoclinic, $C2/c$, a = 17.884(5) Å, b = 12.573(3) Å, c = 23.715(7) Å, β = 107.77(1)°, Z = 4, V = 5077.62 Å^3, R (R_w) = 9.80% (9.37%). The structure of **1** confirms a bis(*gem*-diol) structure with an extended-chain conformation. The anion of **2** consists of two $Mn(hfac)_2$ fragments bridged by the $hfpt^{4-}$ group; the latter functions as a bidentate chelate ligand to each Mn^{III}, employing one alkoxide oxygen atom from each *gem*-diolate pair. Variable-temperature magnetochemical studies have been performed on powdered samples of **2** in the range 5–320 K. THe Mn^{III} centers are weakly interacting; the exchange interaction is ferromagnetic, and fitting of the data leads to the following values for the variables: J = +0.21 cm^{-1} (employing the $-2J\hat{S}_1\cdot\hat{S}_2$ convention), D = 0.9 cm^{-1}, g = 1.99. Vacuum thermolysis of **2** in the range 111–150 °C yields $(py)Mn(hfac)_3$ (**3**) and lesser amounts of *cis*-$Mn(py)_2(hfac)_2$ (**5**), $Mn(hfac)_3$ (**4**), the tetraol (**1**), and a manganese(≥IV) oxide. All but the oxide are volatile and have been characterized in part by single-crystal X-ray diffraction. The mechanism of thermolysis is proposed to be initiated by proton transfer from pyH^+ to the tetraolate oxygen to which it is hydrogen bonded; this process facilitates the electrophilic cleavage of C/O bonds, which furnishes $hfac^-$ as well as oxide for the manganese oxide product. Crystal data for **3** (−175 °C): a = 10.487(2) Å, b = 15.790(4) Å, c = 9.356(2) Å, α = 101.78(1)°, β = 106.58(1)°, γ = 108.50(1)° with Z = 2 in space group $P\bar{1}$. Crystal data for **4** (−159 °C): a = 8.879(0) Å, b = 12.941(1) Å, c = 18.748(1) Å, β = 91.35(0)° with Z = 4 in space group $P2_1/n$. Crystal data for **5**: a = 9.112(3) Å, b = 16.821(6) Å, c = 16.315(5) Å, β = 105.34(5)° with Z = 4 in space group $C2/c$.

Introduction

It has long been known[1] that hexafluoroacetone, $(CF_3)_2CO$, will readily undergo nucleophilic attack at the ketone carbon atom to yield a stable "hydrate", the *gem*-diol hexafluoro-2,2-propanediol, $(CF_3)_2C(OH)_2$. On deprotonation, the latter can function as a dianionic ligand toward both main group[2] and transition metals.[3] Analogous chemistry with hexafluoroacetylacetone (hfacH) has not been investigated. The doubly-hydrated form of hfacH is the bis(*gem*-diol) 1,1,1,5,5,5-hexafluoropentane-2,2,4,4-tetraol ($hfptH_4$, **1**) which has been briefly mentioned as

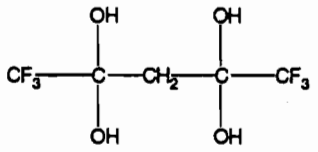

1

a low-yield side product in the preparation of hfacH.[4] However, a convenient high-yield route to **1** has yet to be devised and the ability of its deprotonated form to bind to metals has not been explored to date.

In this paper, we report a particularly straightfoward route to good yields of pure **1** and the initial example of its employment as a ligand. The preparation of $(pyH)_2[Mn_2(hfpt)(hfac)_4]$ (**2**), possessing the deprotonated form of **1** as a tetradentate bridging ligand, is described. We also describe the results of a varible-temperature magnetic susceptibility study designed to establish the sign and magnitude of the magnetic exchange interactions between the Mn^{III} ions mediated by this ligand in the particular bridging mode adopted. A preliminary report of this work has appeared.[5]

Compound **2** contains an unusual mix of functionalities: the proton, the Lewis base pyridine (subsequent to any possible proton transfer), hfac ligands with weakened bonds to manganese due to hydrogen bonding, the unique and sterically compact tetraolate ligand $CF_3C(O)_2CH_2C(O)_2CF_3^{4-}$, and two Jahn–Teller-distorted Mn^{III} centers. In addition, there is the possibility that the two metal centers could operate on the single tetraolate ligand to disassemble it, perhaps by oxide abstraction to give volatile $CF_3C(O)CH_2C(O)CF_3$ and two O^{2-} ions. Finally, given the production of BaF_2 from $Ba(hfac)_2$ under chemical vapor deposition conditions,[6] we anticipated that abstraction of F^- from carbon could take place. To test some of the general principles of reactivity

* To whom correspondence should be addressed: K.G.C. and G.C., Indiana University; D.N.H., University of California at San Diego.

(1) Middleton, W. J.; Lindsey, R. V. *J. Am. Chem. Soc.* **1964**, *86*, 4948.
(2) (a) Prager, J. H.; Ogden, P. H. *J. Org. chem.* **1968**, *33*, 2100. (b) Ogden, P. H.; Nicholson, G. C. *Tetrahedron Lett.* **1968**, 3553.
(3) Bradford, P.; Hynes, R. C.; Payne, N. C.; Willis, C. J. *J. Am. Chem. Soc.* **1990**, *112*, 2647.
(4) Schultz, B. G.; Larsen, E. M. *J. Am. Chem. Soc.* **1949**, *71*, 3250.
(5) Bouwman, E.; Huffman, J. C.; Lobkovsky, E. B.; Christou, G.; Tsai, H.-L.; Hendrickson, D. N. *Inorg. Chem.* **1992**, *31*, 4436.
(6) Purdy, A. P.; Berry, A. D.; Holm, R. T.; Fatemi, M.; Gaskill, D. K. *Inorg. Chem.* **1989**, *28*, 2799.

0020-1669/93/1332-3463$04.00/0

Table I. Crystallographic Data for $hfptH_4$ (**1**), $(pyH)_2[Mn_2(hfpt)(hfac)_4]$ (**2**) $(pyH)Mn(hfac)_3$ (**3**), $Mn(hfac)_3$ (**4**), and *cis*-$Mn(py)_2(hfac)_2$ (**5**)

	1	2	3	4	5
chem formula	$C_5H_6O_4F_6$	$C_{35}H_{18}F_{30}N_2O_{12}Mn_2$	$C_{20}H_9F_{18}NO_8Mn$	$C_{15}H_3F_{18}NO_6Mn$	$C_{20}H_{12}F_{12}O_4Mn$
a, Å	11.108(6)	17.884(5)	10.487(2)	8.879(0)	9.112(3)
b, Å	5.104(3)	12.573(3)	15.790(4)	12.941(1)	16.821(6)
c, Å	14.736(8)	23.715(7)	9.356(2)	18.748(1)	16.315(5)
α, deg			101.78(1)		
β, deg	90.30(2)	107.77(1)	106.58(1)	91.35(0)	105.34(5)
γ, deg			108.50(1)		
V, Å^3	835.44	5077.62	1331.99	2153.74	2411.53
Z	4	4	2	4	4
fw	244.09	1338.36	756.20	676.09	627.24
space grou	$P2_1/n$	$C2/c$	$P\bar{1}$	$P2_1/n$	$C2/c$
T, °C	−171	−130	−175	−159	−145
λ, Å	0.710 69	0.710 69	0.710 69	0.710 69	0.710 69
ρ_{calcd}, g cm^{-3}	1.941	1.751	1.885	2.085	1.728
μ(mol Kα), cm^{-1}	2.3	6.38	6.35	7.7	6.45
R	0.0658	0.0980	0.0715	0.0358	0.0345
R_w	0.0742	0.0937	0.0809	0.0388	0.0389

of this unusual compound, we have investigated the thermal decomposition of compound **2**.

Experimental Section

The synthesis and manipulation of all compounds were carried out in air using materials as received. $[Mn_3O(OAc)_6(py)_3](ClO_4)$ was prepared as described elsewhere.[7] Infrared spectra (KBr) were recorded on a Nicolet 510P FTIR spectrometer.

$CF_3C(OH)_2CH_2C(OH)_2CF_3$, $hfptH_4$ (1). A solution of hfacH (2.0 mL, 14 mmol) in toluene (20 mL) was treated with water (0.51 g, 28 mmol). The two-phase system was maintained at ambient temperature and shaken occasionally to assist reaction. Crystallization of a white solid began after 15 min. When crystallization was judged complete, the solid was collected by filtration, washed copiously with toluene, and dried in air. The yield was 80–85%. Recrystallization can be effected from hot water. Anal. Calcd for $C_5H_6F_6O_4$: C, 24.60; H, 2.48. Found: C, 24.69; H, 2.51. IR data (cm^{-1}): 3390 (vs, broad), 3300 (vs, broad), 1466 (m), 1360 (w), 1275 (s), 1208 (s), 1188 (s), 1138 (vs, broad), 988 (m), 909 (m), 822 (w), 741 (w) 664 (w), 507 (w). ^{1}H NMR (THF-d_8): δ 7.03 (s, OH), 2.16 (s, CH_2). $^{13}C\{^1H\}$ NMR (THF-d_8): δ 123.45 (q, CF_3), 95.52 (q, $C(OH)_2$), 34.08 (s, CH_2). Mass spectrum (EI): m/z 208 (M − $2H_2O$), 156 (M − H_3OCF_3), 139 ($C_4O_2F_3H_2$), 115 ($C_2F_3O_2H_2$), 69 (CF_3).

$(pyH)_2[Mn_2(hfpt)(hfac)_4]$ (2). Pyridine (0.36 g, 4.5 mmol) and $[Mn_3O(OAc)_6(py)_3](ClO_4)$ (0.44 g, 0.50 mmol) were dissolved in CH_2Cl_2 (20 mL), and the solution was filtered. To the filtrate were added $hfptH_4$ (0.18 g, 0.75 mmol), dissolved in a minimum amount of MeCN (0.5 mL), and hfacH (0.42 mL, 3.0 mmol). The dark brown homogeneous solution was stored in a freezer overnight, and the resulting dark brown microcrystalline product was collected by filtration, washed with CH_2Cl_2, and dried in air. The yield was 58%. Anal. Calcd for $C_{35}H_{18}F_{30}N_2O_{12}Mn_2$: C, 31.41; H, 1.36; N, 2.09; Mn, 8.21. Found: C, 31.7; H, 1.5; N, 2.1; Mn, 8.2.

Magnetochemical Studies. The variable-temperature, solid-state magnetic susceptibility of complex **2** was measured on a powdered sample restrained in Parafilm to prevent torquing. Data was collected in the temperature range 5.01–320.00 K employing a SQUID susceptomer (SHE Corp.) and a 10.0-kG applied field. Data were also collected in the range 2.00–30.00 K at 10.0- and 50.0-kG fields. Diamagnetic corrections were estimated using Pascal's constants and subtracted from the experimental susceptibility values to yield the molar magnetic susceptibilities.

Thermolysis Studies. Thermolysis reactions were executed by positioning the loaded borosilicate glass tube (5-mm i.d., 7-mm o.d.) in a tube furnace at room temperature, establishing a vacuum in the tube, and then ramping the furnace to the stated temperature (Figure 1). The maximum time to reach that temperature was 2.5 h. The temperatures stated here are those measured by a thermocouple held directly against the reaction tube at the sample position.

An exploration of the minimum temperature necessary for thermolysis revealed that, at 111 °C, very small quantities of a colorless and a yellow solid were produced. At this "threshold" thermolysis temperature, the transformation was extremely slow, and approximately 90% of complex **2** remained unconverted, in its original, free-flowing, microcrystalline form, after 5 h of total heating. At temperatures of 125 °C, conversion of complex **2** was essentially complete after 5 h total heating time.

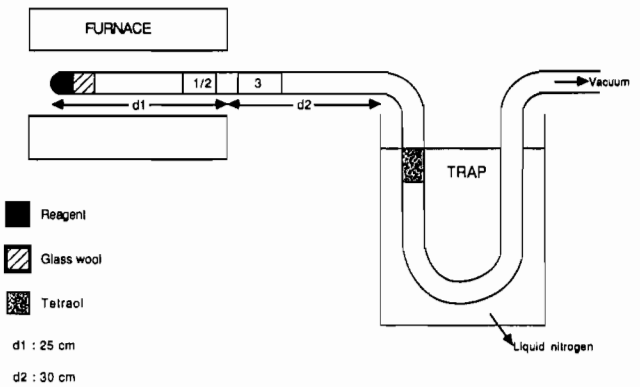

Figure 1. Schematic of the hot-wall thermolysis apparatus, showing zones where products **1**–**3** deposit.

***cis*-$Mn(py)_2(hfac)_2$ (5).** Light yellow $Mn(H_2O)_2(hfac)_2$[8] (0.30 g, 0.59 mmol) was suspended in toluene (10 mL). Pyridine (0.48 mL, 6.0 mmol) was added dropwise, which caused all solid to dissolve and yield a homogeneous orange solution. This solution was stirred for 30 min, concentrated, and cooled to −18 °C overnight. The resulting precipitate was composed of both orange and colorless solids. After filtration of these solids, the orange product was selectively dissolved in a minimum of CH_2Cl_2. Concentration of this solution and cooling at −18 °C overnight gave orange crystals, which were recrystallized by sublimation at 97 °C. Anal. Calcd for $C_{20}H_{12}N_2O_4F_{12}Mn$: C, 38.30; H, 1.93; N, 4.46. Found (synthetic product): C, 37.61; H, 1.85; N, 4.00. Found (thermolysis product): C, 38.29; H, 1.83; N, 4.37.

X-ray Diffraction Structure Determinations. General Details. A suitable crystal was located and was affixed to the end of a glass fiber using silicone grease and transferred to the goniostat where it was cooled for characterization (Table I) and data collection[9] ($6° < 2\theta < 45°$). Data were collected in the usual manner, and after reduction and averaging, direct methods (MULTAN) located the positions of all non-hydrogen atoms.

(a) $CF_3C(OH)_2)CH_2C(OH)_2CF_3$, $hfptH_4$ (1). A final difference Fourier map was featureless, the largest peak being 0.49 e/Å^3. The results of the structure determination are shown in Table II and Figures 2 and 3.

(b) $(pyH)_2[Mn_2(hfpt)(hfac)_4]$ (2). The sample undergoes a phase transition below −130 °C. A final difference Fourier map was featureless, with the largest peak being 0.70 e/Å^3. The results of the structure determination are shown in Table III and Figures 4 and 5.

(c) $(pyH)[Mn(hfac)_3]$ (3). A suitable sample[10] yielded intensities (−175 °C) which refined unexceptionally. A final difference Fourier

(7) Vincent, J. B.; Chang, H.-R.; Folting, K.; Huffman, J. C.; Christou, G.; Hendrickson, D. N. *J. Am. Chem. Soc.* **1987**, *109*, 5703.
(8) Charles, R. G. *Inorg. Synth.* **1960**, *6*, 164.
(9) For general crystallographic methods applied to all structures, see: Huffman, J. C.; Lewis, L. N.; Caulton, K. G. *Inorg. Chem.* **1980**, *19*, 2755.
(10) Anal. Calcd for $C_{20}H_9F_{18}NO_6Mn$: C, 31.79; H, 1.19; N, 1.85. Found: C, 31.88; H, 1.25; N, 1.89.

Table II. Selected Bond Distances (Å) and Angles (deg) for $C_5H_6O_4F_6$ (**1**)

F(2)–C(1)	1.329(9)	O(7)–C(5)	1.404(10)
F(3)–C(1)	1.344(9)	O(10)–C(9)	1.397(9)
F(4)–C(1)	1.334(8)	O(11)–C(9)	1.410(10)
F(13)–C(12)	1.345(9)	C(1)–C(5)	1.530(11)
F(14)–C(12)	1.328(10)	C(5)–C(8)	1.514(12)
F(15)–C(12)	1.343(9)	C(8)–C(9)	1.532(11)
O(6)–C(5)	1.408(9)	C(9)–C(12)	1.532(11)
F(2)–C(1)–F(3)	107.2(6)	O(10)–C(9)–O(11)	111.8(6)
F(2)–C(1)–F(4)	107.6(6)	O(10)–C(9)–C(8)	112.5(7)
F(2)–C(1)–C(5)	111.7(6)	O(10)–C(9)–C(12)	104.7(6)
F(3)–C(1)–F(4)	107.0(6)	O(11)–C(9)–C(8)	107.8(7)
F(3)–C(1)–C(5)	111.0(6)	O(11)–C(9)–C(12)	109.2(7)
F(4)–C(1)–C(5)	112.0(6)	C(8)–C(9)–C(12)	110.7(7)
O(6)–C(5)–O(7)	111.6(6)	F(13)–C(12)–F(14)	108.4(6)
O(6)–C(5)–C(1)	109.5(6)	F(13)–C(12)–F(15)	107.2(7)
O(6)–C(5)–C(8)	107.2(7)	F(13)–C(12)–C(9)	111.1(6)
O(7)–C(5)–C(1)	104.2(6)	F(14)–C(12)–F(15)	107.2(6)
O(7)–C(5)–C(8)	114.3(7)	F(14)–C(12)–C(9)	112.3(7)
C(1)–C(5)–C(8)	109.9(6)	F(15)–C(12)–C(9)	110.4(7)
C(5)–C(8)–C(9)	113.3(7)		

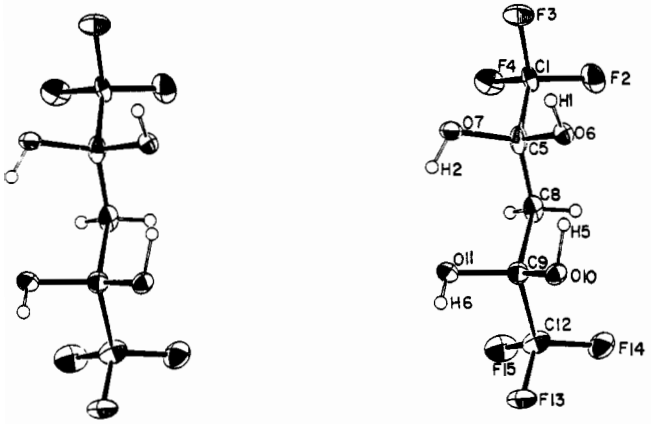

Figure 2. Stereo ORTEP drawing of $CF_3C(OH)_2CH_2C(OH)_2CF_3$.

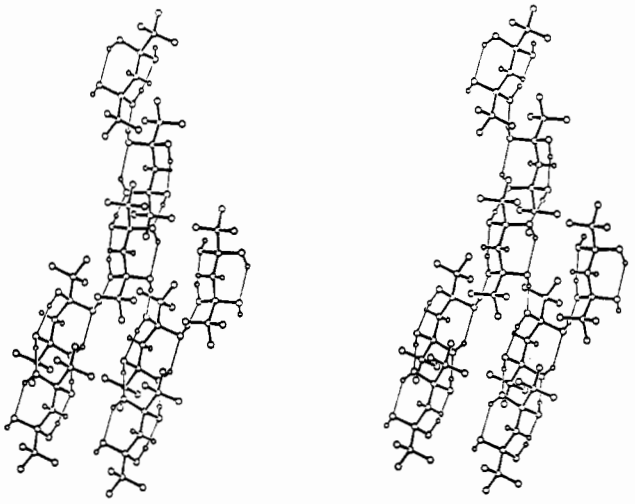

Figure 3. Stereo ORTEP drawing of the network of intra- and intermolecular hydrogen bonds in solid $CF_3C(OH)_2CH_2C(OH)_2CF_3$.

map was featureless, with maximum and minimum peaks of +0.77 and −0.76 e/Å^3. No absorption correction was performed. The results of the structure determination are shown in Table IV and Figure 6.

(d) Mn(hfac)$_3$ (4). The final difference Fourier map was essentially featureless, the maximum and minimum electron densities being 0.38 and −0.43 e/Å^3, respectively. The results of the structure determination are shown in Table V and Figure 7.

(e) *cis*-Mn(py)$_2$(hfac)$_2$ (5). The final difference Fourier map was essentially featureless, with the largest peaks being 0.84 e/Å^3 between the Mn and O atoms and 0.70 e/Å^3 in the vicinity of the fluorine atoms of the hfac ligand. The results are shown in Table VI and Figure 8.

Table III. Selected Bond Distances (Å) and Angles (deg) for $(pyH)_2[Mn_2(hfpt)(hfac)_4]$ (**2**)

Mn(1)–O(17)	1.875(7)	O(17)–C(23)	1.393(13)
Mn(1)–O(18)	1.859(8)	O(18)–C(23)	1.372(13)
Mn(1)–O(19)	2.017(7)	O(19)–C(27)	1.259(12)
Mn(1)–O(20)	2.219(8)	O(20)–C(29)	1.263(13)
Mn(1)–O(21)	1.972(7)	O(21)–C(32)	1.278(13)
Mn(1)–O(22)	2.228(8)	O(22)–C(34)	1.202(12)
O(17)–Mn(1)–O(18)	94.4(3)	O(18)–Mn(1)–O(22)	95.2(3)
O(17)–Mn(1)–O(19)	175.8(3)	O(19)–Mn(1)–O(20)	84.0(3)
O(17)–Mn(1)–O(20)	96.3(3)	O(19)–Mn(1)–O(21)	87.3(3)
O(17)–Mn(1)–O(21)	88.6(3)	O(19)–Mn(1)–O(22)	86.3(3)
O(17)–Mn(1)–O(22)	92.7(3)	O(20)–Mn(1)–O(21)	83.1(3)
O(18)–Mn(1)–O(19)	89.6(3)	O(20)–Mn(1)–O(22)	165.55(28)
O(18)–Mn(1)–O(20)	95.4(3)	O(21)–Mn(1)–O(22)	85.8(3)
O(18)–Mn(1)–O(21)	176.7(3)		

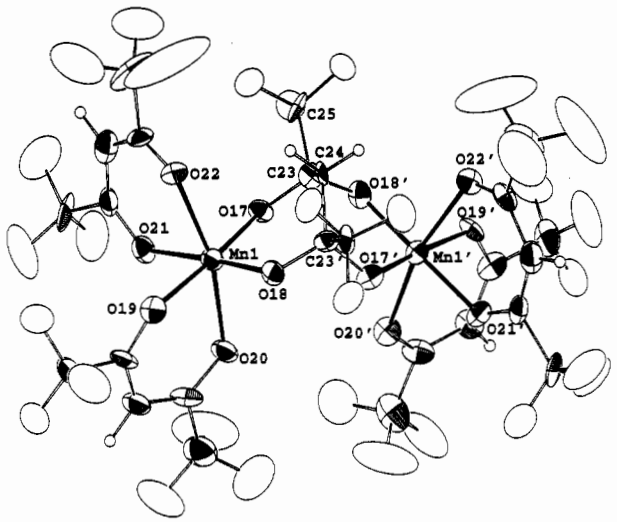

Figure 4. ORTEP drawing of the anion of $(pyH)_2[Mn_2(hfpt)(hfac)_4]$ (**2**). Primed and unprimed atoms are related by the C_2 axis through C(24).

Results

Syntheses and Structures of 1 and 2. Complex **2** was originally observed as a low-yield product in the reaction of $[Mn_3O(OAc)_6(py)_3](ClO_4)$ with hfacH. Having previously observed that acac$^-$ is too good a reducing agent for use with this Mn_3O reagent, we had switched to hfac$^-$, whose electron-withdrawing CF_3 groups increase resistance to oxidation. The observation of hfpt^{4-} on crystallographic identification of the product was a surprise; it can be rationalized as a consequence of activation by the CF_3 groups of the ketonic carbon atoms to nucleophilic attack, but the precise mechanism of formation of **2** is unclear.

Complex **2** was sufficiently novel to warrant the development of a rational synthesis. We also recognized the potential general interest in, and applications of, this new tetraolate ligand. The parent molecule has long been known; it had been observed by Schultz and Larsen in 1949 as a low-yield, crystalline side product in the preparation of hfacH,[4] but it appears that its use as a ligand has never been explored. The first requirement was a high-yield synthesis of the tetraol (**1**). Schultz and Larsen had observed that treatment of an ethereal solution of hfacH with a little water gave a negative test for the diketone (no green color with copper(II) acetate), suggesting formation of the doubly-hydrated molecule, *viz.* $hfptH_4$ (**1**). Using this observation, a preparative-scale synthesis of **1** has been devised involving treatment of hfacH with H_2O in toluene, in which the product is insoluble. This leads to high-yield isolation of **1**, whose bis(*gem*-diol) identity was confirmed by X-ray crystallography after recrystallization from hot water. Its structure is described in Table II and Figures 2 and 3. The structure was also deemed important for future reference since the tetraol is a polyfunctional

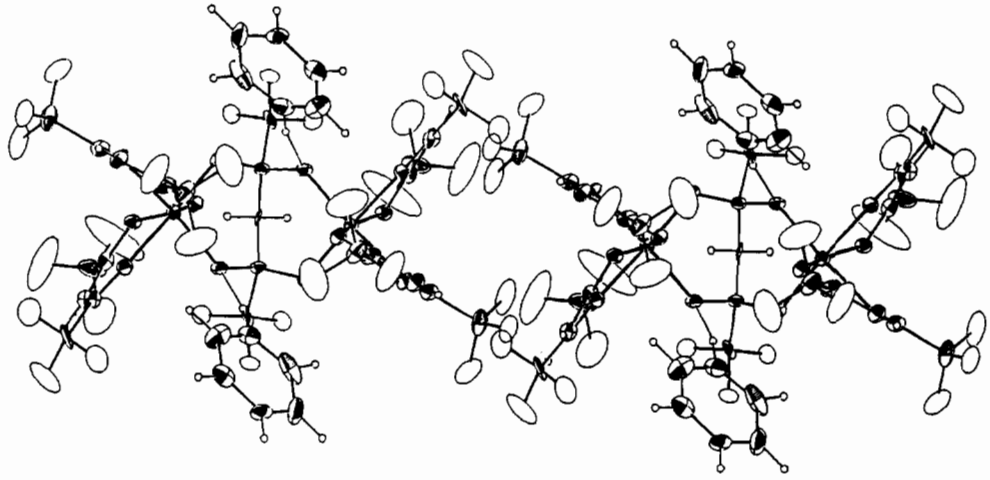

Figure 5. Stereo ORTEP drawing of **2** showing the hydrogen bonding between the anion and the pyH^+ cations. The view is approximately along the C_2 axis.

Table IV. Selected Bond Distances (Å) and Angles (deg) for $(pyH)Mn(hfac)_3$ (**3**)

Mn(1)–O(2)	2.139(6)	C(3)–C(4)	1.384(13)
Mn(1)–O(6)	2.139(5)	C(3)–C(7)	1.547(12)
Mn(1)–O(15)	2.158(6)	C(4)–C(5)	1.408(12)
Mn(1)–O(19)	2.148(6)	C(5)–C(11)	1.520(13)
Mn(1)–O(28)	2.163(5)	C(16)–C(17)	1.385(12)
Mn(1)–O(32)	2.196(6)	C(16)–C(20)	1.521(12)
O(32)–N(46)	2.934(12)	C(17)–C(18)	1.404(12)
O(2)–C(3)	1.255(10)	C(18)–C(24)	1.523(12)
O(6)–C(5)	1.240(10)	C(29)–C(30)	1.375(12)
O(15)–C(16)	1.267(10)	C(29)–C(33)	1.527(12)
O(19)–C(18)	1.257(9)	C(30)–C(31)	1.400(12)
O(28)–C(29)	1.268(10)	C(31)–C(37)	1.480(13)
O(32)–C(31)	1.278(10)		
O(2)–Mn(1)–O(9)	83.27(21)	O(15)–Mn(1)–O(32)	94.93(22)
O(2)–Mn(1)–O(15)	85.24(21)	O(19)–Mn(1)–O(28)	85.38(21)
O(2)–Mn(1)–O(19)	167.58(22)	O(19)–Mn(1)–O(32)	94.84(22)
O(2)–Mn(1)–O(28)	106.81(21)	O(28)–Mn(1)–O(32)	82.46(21)
O(2)–Mn(1)–O(32)	84.64(21)	Mn(1)–O(2)–C(3)	129.1(5)
O(6)–Mn(1)–O(15)	100.16(22)	Mn(1)–O(6)–C(5)	128.3(5)
O(6)–Mn(1)–O(19)	100.41(21)	Mn(1)–O(15)–C(16)	128.5(5)
O(6)–Mn(1)–O(28)	85.58(21)	Mn(1)–O(19)–C(18)	129.7(5)
O(6)–Mn(1)–O(32)	159.77(21)	Mn(1)–O(28)–C(29)	125.1(5)
O(15)–Mn(1)–O(19)	82.44(21)	Mn(1)–O(32)–C(31)	125.9(5)
O(15)–Mn(1)–O(28)	167.29(21)		

ligand and it also incorporates sufficient CF_3 groups to increase the volatility of metals to which it is attached. The molecule exists in an extended-chain conformation (Figure 2) with substituents staggered about all single bonds. All hydrogens were located, and they confirm that C8 is a methylene group. All C/C, C/O, and C/F distances are consistent with normal single bonds. All C/F bonds are identical to within 2σ. Bond angles involving the refined hydrogen positions are in the range 106(5)–111(8)°. When the hydroxyl hydrogens are considered, the molecule has a noncrystallographic C_2 axis of symmetry bisecting the C(5)–C(8)–C(9) angle. Two of the hydrogens (H(5) and H(2)) are directed inward toward the oxygen of a neighboring hydroxyl group. The O···O separations in these intramolecular hydrogen bonds are 2.690 and 2.695 Å. In addition, the two hydroxyl hydrogens that are directed "outward" form a chain polymeric network of intermolecular hydrogen bonds (Figure 3). Oxygen–oxygen distances in these hydrogen bonds range from 2.741 to 2.802 Å.

With pure tetraol **1** available a rational synthesis of **2** was devised employing the Mn:hfacH;$hfptH_4$ ratio (2:6:1) of the required product and an excess of pyridine. Satisfactory yields (55–60%) are available by this procedure, which continues to employ $[Mn_3O(OAc)_6(py)_3](ClO_4)$ as a convenient source of Mn^{III}.

The structure of the anion of **2** is shown in Figure 4. The anion has crystallographically-imposed C_2 symmetry, the rotation axis passing through the central carbon atom (C(24)) of the $hfpt^{4-}$ ligand. The bridging tridentate $hfpt^{4-}$ ligand occupies two sites at each octahedral Mn^{III} center, the other sites being occupied by $hfac^-$ ligands in their familiar bidentate chelating modes. The Mn^{III} atoms are six-coordinate and demonstrate the Jahn–Teller distortion expected for a high-spin d^4 metal in near-octahedral geometry; axial elongation is clearly evident with Mn(1)–O(20) and Mn(1)–O(22) distances (2.219(8) and 2.228(8) Å, respectively) significantly longer than the rest (1.859(8)–2.017(7) Å). The $hfpt^{4-}$ ligand bridges such that one alkoxide oxygen from each *gem*-diolate pair is attached to a particular Mn^{III} atom; thus, two six-membered chelate rings are formed, and the alkoxide

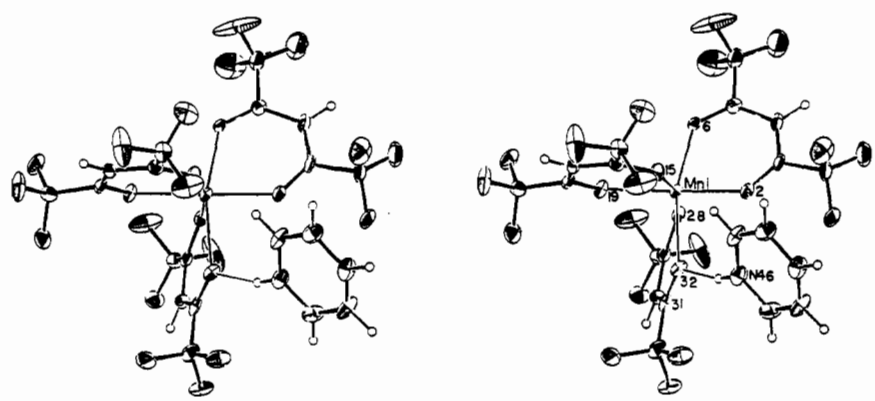

Figure 6. Stereo ORTEP drawing of the ion pair $(pyH)Mn(hfac)_3$, showing hydrogen bonding (O(32)···N(46)) and selected atom labeling. Unlabeled atoms are carbon or (if terminal) fluorine. Open circles are hydrogens.

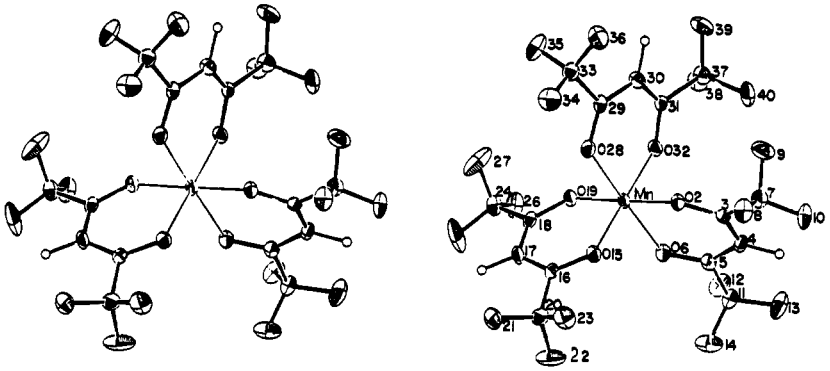

Figure 7. ORTEP drawing of $Mn(hfac)_3$, viewed down a pseudo-3-fold axis of symmetry. The long Mn–O bonds involve O(6) and O(28).

Table V. Selected Bond Distances (Å) and Angles (deg) for $Mn(hfac)_3$ (**4**)

Mn(1)–O(2)	1.9121(25)	C(3)–C(4)	1.369(5)
Mn(1)–O(6)	2.1410(25)	C(3)–C(7)	1.517(5)
Mn(1)–O(15)	1.9327(24)	C(4)–C(5)	1.401(5)
Mn(1)–O(19)	1.9372(25)	C(5)–C(11)	1.531(5)
Mn(1)–O(28)	2.1469(25)	C(16)–C(17)	1.385(5)
Mn(1)–O(32)	1.9063(24)	C(16)–C(20)	1.527(5)
O(2)–C(3)	1.285(4)	C(17)–C(18)	1.383(5)
O(6)–C(5)	1.246(4)	C(18)–C(24)	1.520(5)
O(15)–C(16)	1.264(4)	C(29)–C(30)	1.413(5)
O(19)–C(18)	1.270(4)	C(29)–C(33)	1.539(5)
O(28)–C(29)	1.240(4)	C(30)–C(31)	1.366(5)
O(32)–C(31)	1.282(4)	C(31)–C(37)	1.528(5)
O(2)–Mn(1)–O(6)	87.71(10)	O(2)–C(3)–C(4)	128.5(3)
O(2)–Mn(1)–O(15)	90.54(1)	O(2)–C(3)–C(7)	111.5(3)
O(2)–Mn(1)–O(19)	178.58(10)	C(4)–C(3)–C(7)	120.0(3)
O(2)–Mn(1)–O(28)	89.92(10)	C(3)–C(4)–C(5)	122.0(4)
O(2)–Mn(1)–O(32)	88.70(1)	O(6)–C(5)–C(4)	127.1(3)
O(6)–Mn(1)–O(15)	88.86(10)	O(6)–C(5)–C911)	113.9(3)
O(6)–Mn(1)–O(19)	93.49(10)	C(4)–C(5)–C(11)	119.0(3)
O(6)–Mn(1)–O(28)	177.62(10)	O(15)–C(16)–C(17)	127.3(3)
O(6)–Mn(1)–O(32)	91.71(10)	O(15)–C(16)–C(20)	113.4(3)
O(15)–Mn(1)–O(19)	90.26(10)	C(17)–C(16)–C(20)	119.1(3)
O(15)–Mn(1)–O(28)	91.01(10)	C(16)–C(17)–C(18)	120.9(3)
O(15)–Mn(1)–O(32)	179.03(11)	O(19)–C(18)–C(17)	126.8(3)
O(19)–Mn(1)–O(28)	88.89(10)	O(19)–C(18)–C(24)	113.0(3)
O(19)–Mn(1)–O(32)	90.48(10)	C(17)–C(18)–C(24)	120.2(3)
O(28)–Mn(1)–O(32)	88.39(10)	O(28)–C(29)–C(30)	126.2(3)
Mn(1)–O(2)–C(3)	127.26(23)	O(28)–C(29)–C(33)	116.2(3)
Mn(1)–O(6)–C(5)	123.65(23)	C(30)–C(29)–C(33)	117.5(3)
Mn(1)–O(15)–C(16)	126.93(24)	C(29)–C(30)–C(31)	122.5(4)
Mn(1)–O(19)–C(18)	126.92(23)	O(32)–C(31)–C(30)	129.0(3)
Mn(1)–O(28)–C(29)	123.64(22)	O(32)–C(31)–C(37)	111.4(3)
Mn(1)–O(32)–C(31)	126.31(22)	C(30)–C(31)–C(37)	119.6(3)

Table VI. Selected Bond Distances (Å) and Angles (deg) for *cis*-$Mn(py)_2(hfac)_2$ (**5**)

Mn(1)–O(2)	2.1508(22)	C(3)–C(7)	1.524(5)
Mn(1)–O(6)	2.2221(22)	C(4)–C(5)	1.393(4)
Mn(1)–N(15)	2.2400(26)	C(5)–C(11)	1.525(5)
O(2)–C(3)	1.259(4)	C(16)–C(17)	1.385(5)
O(6)–C(5)	1.245(4)	C(17)–C(18)	1.376(5)
N(15)–C(16)	1.340(4)	C(18)–C(19)	1.368(5)
N(15)–C(20)	1.339(4)	C(19)–C(20)	1.386(5)
C(3)–C(4)	1.381(5)		
O(2)–Mn(1)–O(2)′	175.60(12)	O(6)–Mn(1)–N(15)′	164.70(9)
O(2)–Mn(1)–O(6)	80.90(8)	N(15)–Mn(1)–N(15)′	99.47(13)
O(2)–Mn(1)–O(6)′	95.69(8)	Mn(1)–O(2)–C(3)	128.76(20)
O(2)–Mn(1)–N(15)	95.36(9)	Mn(1)–O(6)–C(5)	126.42(20)
O(2)–Mn(1)–N(15)′	87.49(9)	Mn(1)–N(15)–C(16)	119.52(21)
O(6)–Mn(1)–O(6)′	79.81(12)	Mn(1)–N(15)–C(20)	123.25(21)
O(6)–Mn(1)–N(15)	91.54(9)		

oxygens are all *terminally* coordinated. The latter results in Mn(1)–O(17) and Mn(1)–O(18) (1.875(7) and 1.859(8) Å, respectively) being shorter than Mn(1)–O(19) and Mn(1)–O(21) (2.017(7) and 1.972(7) Å, respectively), as expected for terminal Mn–alkoxide *vs* Mn–diketonate bonds. The two Mn^{III} equatorial planes form a dihedral angle of 137.7°. The saturated nature of the bridging ligand is supported by C–C (1.522(14), 1.547(16) Å) and C–O (1.372(13), 1.393(13) Å) distances that are consistent with single bonds (1.514(12), 1.532(11), and 1.397(9)–1.410(10) Å, respectively, in **1**). The pyH^+ cations are associated with the anion in the solid state; they are hydrogen-bonded to O(17) and O(17)′ with N–H···O distances of 2.74 Å. The stereoview in Figure 5 shows the hydrogen-bonding arrangement in the complete anion/cation assembly.

Magnetochemical Studies. Variable-temperature solid-state magnetic susceptibility studies have been performed on powdered samples of complex **2** (restrained in Parafilm to prevent torquing) in the temperature range 5–320 K in order to characterize the sign and magnitude of the magnetic exchange interaction propagated by this unusual bridging ligand. The effective magnetic moment, μ_{eff}, per Mn_2 molecule rises slightly from 6.73 μ_B at 320 K to a maximum of 6.75 μ_B at 70.0 K, whereupon there is a gradual decrease to 6.67 μ_B at 20 K, followed by a more rapid decrease to 5.96 μ_B at 5.01 K (Figure 9A). A full-matrix diagonalization approach including magnetic exchange ($2J\hat{S}_1\cdot\hat{S}_2$), axial single-ion zero-field ($D\hat{S}_z^2$), and isotropic Zeeman interactions was employed to fit the data. A least-squares fit was found with $J = +0.35$ cm^{-1}, $D = 0.9$ cm^{-1}, and $g = 1.94$. The solid line in Figure 9A shows the quality of this fit, which can be seen to be good. The fitting parameters were checked by collecting additional data at both 10.0 and 50.0 kG in the 2.00–30.0 K range. These two data sets were fit together to give $J = +0.21$ cm^{-1}, $D = 0.9$ cm^{-1}, and $g = 1.99$ (Figure 9B). Thus, we conclude there is a *very* weak ferromagnetic exchange interaction between the Mn^{III} ions of complex **2**, with a resulting $S = 4$ ground state. This result is consistent with the particular bridging mode adopted and the large Mn···Mn distance (4.641(5) Å).

Thermolysis Studies. Thermal decomposition of **2** was carried out under vacuum (10 mTorr base pressure) in the apparatus shown in Figure 1. The sample was heated to ~125 °C near the furnace edge. The sample was separated from the central zone of the furnace by a tightly packed pad of glass wool (length ~4 cm). Preliminary runs without glass wool exhibited the same behavior. It was found advantageous to leave a considerable length of postreactor surface (d2) at ambient temperature to collect *and fractionate* products of moderate volatility. Highly volatile products were collected at −196 °C in a U-trap filled with glass beads.

The oven temperature was chosen to be only slightly (<20 °C) above the lowest temperature at which thermal decomposition occurs, in an effort to avoid further thermolysis of primary products and also to avoid "flooding" the product collection zone (d2) and thereby degrading the fractionation of the various products in that region. The complex thermolysis behavior reported here was found to be reproducible over about 30 runs. Thermolysis behavior was found to be similar up to ~155 °C. Under these conditions, it was found that metal-containing products of three different morphologies and colors collected: a yellow product in zone **1**, an orange product in zone **2**, and a dark brown product

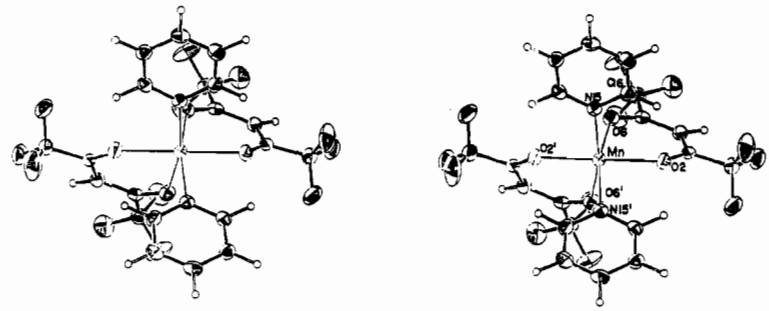

Figure 8. Stereo ORTEP drawing of *cis*-$Mn(py)_2(hfac)_2$, viewed down the crystallographic C_2 axis. Primed and unprimed atoms are related by this C_2 axis, and unlabeled atoms follow the numerical sequence shown.

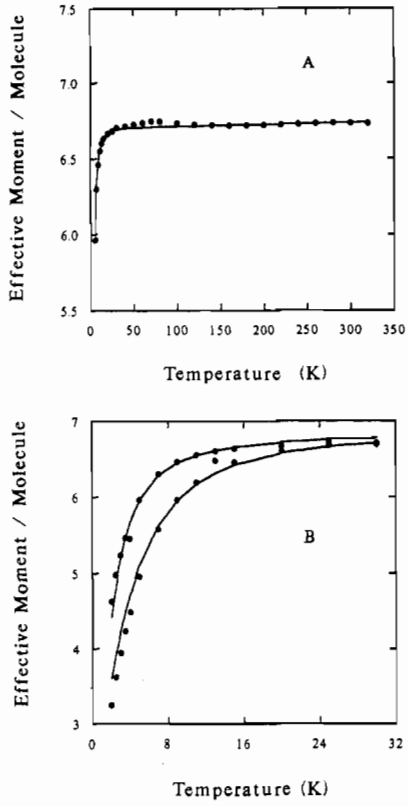

Figure 9. Calculated (lines) and experimental (points) temperature dependence of the magnetic moment of **2** (A) over a broad temperature range and (B) at low temperature and two field strengths. See text for fitting parameters.

in zone 3. There was also, throughout region d2, a thin coating of a very small amount of a colorless solid.[11] The amount of products varied according to yellow > orange > brown > colorless, which is consistent with the observation of no brown or orange product at 111 °C. In these runs, the consumption of reagent **2** was complete, and only a small amount of black solid remained in the reagent zone, together with some oily residue. The black solid tested positive for manganese (acidic periodate oxidation yielded permanganate) and may be MnO_2.

In every thermolysis run, the appearance of the reaction tube downstream from the sample/glass wool zone but still within the tube furnace was essentially colorless and free of any deposit. Given the low pressure, the straight geometry, and the lack of deposit within the furnace, we conclude that all of the thermolysis chemistry occurs within the sample reservoir zone. Only here is there effective heat transfer to the sample molecules, and thus (given the low volatility of reagent **2**) both heat transfer and the resultant chemical reaction occur primarily in the solid state.

Product 1, (pyH)Mn(hfac)$_3$ (3). The major thermolysis product is a yellow crystalline material which collected closest to the reagent reservoir (zone 1) but which showed intergrowth with zone 2. The quality of crystals direct from a thermolysis was poor so the zone 1/2 products were washed from the reactor walls with CH_2Cl_2 and recrystallized by slow evaporation of that solvent, to give a mixture of yellow and orange crystals, from which a yellow one suitable for structure determination was selected. A single-crystal X-ray diffraction study revealed that the yellow product is (pyH)[Mn(hfac)$_3$] (Figure 6). Reduction of manganese has occurred. The [Mn(hfac)$_3$]$^-$ portion of the structure is a tris-chelate moiety with five identical ($\pm 2\sigma$) Mn–O distances (average value 2.149 Å). The pyridinium cation is not an "innocent" counterion but is involved in a hydrogen bond to one oxygen (O(32)) coordinated to manganese(II).[12] The N(46)···O(32) distance is 2.934(12) Å, and the hydrogen bond has the effect of lengthening that Mn–O(32) bond to 2.196(6) Å, which is 9σ (0.046 Å) longer than the average of the other five Mn–O distances; hydrogen bonding decreases the donor power of the chelate oxygen. The chelate ring involved in hydrogen bonding is distinctly folded along the O(28)···O(32) line, in contrast to the other two, which are coplanar with the metal. Finally, the O(32)–C(31) distance, at 1.278(10) Å, is the longest of the six C/O distances, although it is only 2σ longer than the average of the other five values. The average of six Mn^{II}/O distances, 2.157 Å, is considerably longer than the average Mn^{III}/O distance in Mn(hfac)$_3$ (1.996 Å) (see below).

The occurrence of hydrogen bonding in the solid state (to give a zwitterionic intimate ion pair) is certainly relevant to the volatility of this compound. That is, this ion pairing will persist in the vapor phase, giving an uncharged species of moderate molecular weight, which is thus subject to vapor transport.

When (pyH)[Mn(hfac)$_3$] is subjected to the standard thermolysis conditions (125 °C in a clean glass tube), all of its survives unchanged. Thus, this compound is not the source of the orange and brown products by a secondary thermolysis reaction.

Product 2, *cis*-Mn(py)$_2$(hfac)$_2$ (5). Zone 2 collected a product which was first identified by X-ray diffraction (Figure 8) after recrystallization and mechanical separation from **3**. This compound was then also synthesized independently, from reaction of *trans*-$Mn(H_2O)_2(hfac)_2$ with excess pyridine in toluene at 25 °C. Orange solid was obtained by concentration and cooling. Orange crystals were obtained by recrystallization from CH_2Cl_2. The "synthetic" molecule (recrystallized by sublimation at 97 °C) was shown to be identical to the thermolysis product by elemental analysis and cell constant determination.

The molecule has a crystallographic C_2 axis bisecting the N–Mn–N angle, and the two independent Mn–O distances differ considerably, with that *trans* to nitrogen (2.22 Å) being considerably longer than that *trans* to oxygen of a second hfac ligand (2.15 Å). The pyridine plane eclipses two Mn/O bonds. It is the molecular dipole moment which is responsible for this molecule being less volatile than compound **4**.

(11) This colorless solid is insoluble in hydrocarbon solvents and is thought to be a fluorocarbon polymer.

(12) The cesium analog, $CsMn(hfac)_3$, has been reported: Gurevich, M. Z.; Sas, T. M.; Mazepova, N. E.; Zelentsov, V. V.; Stepin, B. D. *Russ. J. Inorg. Chem.* (*Engl. Transl.*) **1975**, *20*, 412.

It should be noted that the seemingly analogous *cis*-Mn(*o*-phenanthroline)(acac)$_2$[13] has an Mn–N distance of 2.307(5) Å and that the Mn–O distances *trans* (2.116(5) Å) and *cis* (2.152(5) Å) to nitrogen are much more similar to each other than they are in *cis*-Mn(py)$_2$(hfac)$_2$. This change from Mn(py)$_2$(hfac)$_2$ represents an inversion of bond lengths in the MnN_2O_2 plane, from long Mn–N/short Mn–O to short Mn–N/long Mn–O.

This compound was subjected to thermolysis in vacuum to explore the possibility that it could be isomerized to a *trans* isomer. There was no evidence for change after 2 h at 160 °C or even 2 h at 200 °C. Finally, after 2 h at 210 °C, it decomposed to a black residue.

Product 3, Mn(hfac)$_3$ (4). The most volatile (zone 3) product was deep brown and formed as microcrystalline rosettes (together with some very small single crystals) and a small amount of dark brown film. In order to obtain crystals suitable for identification by single-crystal X-ray diffraction, this product was sealed under vacuum inside a clean glass tube and subjected to a small (10–30 °C) temperature differential over the 10-cm length of the tube. This led to growth of dark brown single crystals. The lowest sublimation temperatures (~35 °C) yielded the largest crystals. These were identified as Mn(hfac)$_3$ by X-ray diffraction (Figure 7). The solid is well-ordered and shows one O–Mn–O axis of the octahedron to be significantly elongated compared to the other two. The long (*trans*) Mn–O distances are 2.141(3) and 2.147(3) Å, while the other four distances range from 1.906(2) Å to 1.937(3) Å. This is a large distinction (nearly 0.25 Å) among Mn/O distances and is attributed to the Jahn–Teller effect of the high-spin d^4 configuration in near-octahedral geometry. The C/O distances involving the weakly bonded oxygens (O(6) and O(28)) are slightly shorter than the other four examples. The remaining metric parameters are unexceptional. Note that Mn(acac)$_3$ has been crystallized in at least two polymorphs, one[14] which is axially elongated (as Mn(hfac)$_3$ here) and one[15] which is axially *compressed*. Neither is isomorphous with the Mn(hfac)$_3$ reported here. Mn(hfac)$_3$ has a high density (2.085 g/cm^3) due to the high fluorine content. The periphery of the molecule is highly fluorinated, and intermolecular repulsion among fluorine lone pairs contributes to the high volatility of this molecule.

Cold-Trap Contents. The contents of the −196 °C trap were shown (^{1}H and ^{13}C NMR in THF-d_8 and mass spectrum) to be exclusively the tetraol, $CF_3C(OH)_2CH_2C(OH)_2CF_3$. Spectra were compared to that of an authentic sample (see Experimental Section), which was also characterized by a single-crystal structure determination. No pyridine was found in the trap.

When the tetraol itself was subjected to the standard thermolysis conditions (125 °C) in a clean glass tube, all of it survived unchanged and was collected in the −196 °C trap.

Discussion

Synthesis. The convenient preparation of **1** in a single-step, high-yield reaction employing commercially-available hfacH provides access to adequate quantities for a detailed exploration of its ligation properties. In complex **2** it adopts a bridging tetradentate ligation mode, but other modes are clearly possible. We have elsewhere,[5] for example, reported that with Fe^{III} it forms the mononuclear complex (pyH)[Fe(hfptH$_2$)(hfac)$_2$], in which a bidentate chelating mode is adopted with two oxygen atoms remaining protonated and not bound to the Fe^{III}. There is little doubt that hfptH$_4$ will prove to be a useful and versatile ligand for a number of future applications and with a variety of metals.

Magnetism. The particular ligation mode exhibited by hfpt^{4-} in **2** leads to weak ferromagnetic exchange interactions between the Mn^{III} centers. This result is not surprising, given the bridging mode adopted (i.e., the alkoxide oxygens are all bound in a terminal fashion) and the saturated nature of the hfpt^{4-} ligand, which enforces orthogonality of the Mn^{III} magnetic orbitals. Also, the Mn···Mn distance (4.641(5) Å) is much too long for any direct through-space overlap of the magnetic orbitals. Thus, the extreme weakness and the positive sign of the exchange interaction are reasonable on the basis of the observed structure of **2**. It is also clear, however, that hfpt^{4-} could also support antiferromagnetic exchange interactions; for example, if an individual alkoxide oxygen were bridging metal centers rather than being coordinated terminally, then the exchange interaction could reasonably be expected to be antiferromagnetic and also to be much stronger than observed for **2**. Thus, future magnetochemical studies of hfpt^{4-} complexes with various paramagnetic metals and nuclearities ≥2 will likely prove very instructive.

Thermolysis Behavior. Due to the small scale of the thermolysis reactions and the incomplete separation of the product metal complexes, a complete material balance could not be obtained. However, certain conclusions are possible concerning the thermolytic reactivity of the Mn^{III}/tetraolate complex.

(1) The identification of two products as containing Mn^{II} supports our contention that the black, nonvolatile residue remaining in the reactant chamber is MnO_2 (or some oxide of Mn^{IV} or higher). The implied disproportionation of Mn^{III} is attractive as the source of reduced manganese since we feel that hfac is too electron-poor an organic moiety to serve as a reducing agent.

(2) Since two products contain three hfac ligands per Mn (i.e., they are richer in hfac than is the reagent, of empirical formula "(pyH)Mn(hfac)$_2$(tetraolate)$_{0.5}$"), there must also be a product which is poorer in hfac. The nonvolatile manganese oxide residue fills this requirement.

(3) No metal-containing product contains a tetraolate ligand. This is conistent with some degree of removal of O^{2-} nucleophile from the tetraolate. A reaction which simultaneously generates some of the hfac needed in item 2 above is the formal (metal-assisted) reaction in eq 1. The generated O^{2-} and OH^- will

$$CF_3C(O)_2CH_2C(O)_2CF_3^{4-} \rightarrow CF_3C(O)CHC(O)CF_3^- + O^{2-} + OH^- \quad (1)$$

contribute to the formation of the MnO_2 residue. It is noteworthy that pyH$^+$ is hydrogen-bonded to two of the four tetraolate oxygens in reagent **2**. This (together with the tetraolate bond to Mn^{III} in **2**) provides ample electrophilic activation for heterolytic rupture of some C/O bonds of the tetraolate in **2**. It is also relevant that equilibrium 2 is reversible. Protons are clearly capable of splitting C/O bonds in the tetraol.

$$H(hfac) + 2H_2O \rightleftarrows \text{tetraol} \quad (2)$$

(4) The protons of OH^- and of some of the pyH$^+$ (which furnishes the pyridine found in Mn(py)$_2$(hfac)$_2$) will enable the formation of neutral tetraol, which is found in the −196 °C trap. Both Mn(py)$_2$(hfac)$_2$ and Mn(hfac)$_3$ are depleted in protons relative to **2** and thus represent species which balance the four protons needed to make one tetraol molecule.

(5) The material balance in pyridine (which is *not* found in the −196 °C trap) is satisfactorily accommodated since Mn(hfac)$_3$ and Mn(py)$_2$(hfac)$_2$ are respectively poor and rich in pyridine relative to the 1:1 ratio in **2**. These two products are formed in comparable amounts. Since no pyridine is found in the −196 °C trap, this Lewis base is very efficiently trapped when pyH$^+$ is deprotonated within the solid state.

Conclusion

The described convenient synthesis of **1**, its polyfunctional and fluorinated nature, and the establishment of its ability to act as

(13) Stephens, F. S. *Acta Crystallogr.* **1977**, *B33*, 3492.
(14) Stults, B. R.; Marianelli, R. S.; Day, V. W. *Inorg. Chem.* **1979**, *18*, 1853.
(15) Fackler, J. P.; Avdeef, A. *Inorg. Chem.* **1974**, *13*, 1869.

a metal-binding ligand undoubtedly presage a rich new area of study for this tetraol(ate) ligand. Its tetraanionic nature on complete deprotonation coupled with its resistance to oxidation suggests one future application to be as a stabilizing ligand for higher oxidation state metal ions that are good oxidizing agents (e.g., Mn^{III}). The thermolytic behavior of this ligand consists of low-temperature scission of one of each of the geminal C–O bonds but retention of all C–C and C–F bonds of the resultant hfac ligand. The fluorinated tetraolate ligand thus serves to enhance volatility and smoothly delivers oxide ions. This combination should be useful in metal ion transport and deposition of metal oxides.

The solid-state chemistry that evolves on heating **2** is probably initiated by the most kinetically mobile constituents of the unit cell: the protons. Their electrophilic character facilitates C/O bond cleavage (leading to hfac and Mn/oxo bonds) and simultaneously releases the nucleophile pyridine, which effects ligand (hfac) substitution chemistry. Considering the complexity of the observed array of products, this seems to provide a reasonable level of understanding of the thermolysis chemistry of compound **2**. At the same time, it implies that a metal (e.g., alkali metal or alkaline earth metal) or an R_4E^+ (E = N, P) counterion might considerably alter the thermolysis reactivity.

Acknowledgment. This work was supported by DOE Grant DE-FG02-88-ER13906, by NIH Grant GM39083, and by NATO (E.B.). We thank Sheyi Wang for providing samples and for help with figure preparation.

Supplementary Material Available: Tables giving full crystallographic parameters, anisotropic thermal parameters, fractional coordinates and isotropic thermal parameters, and magnetic susceptibility data (10 pages). Ordering information is given on any current masthead page.